DETERMINATION OF FRACTURE TOUGHNESS AND STRAIN ENERGY RELEASE RATE FOR BASALT/EPOXY COMPOSITES

CHANDRESHAH LAL

MECHANICAL ENGINEERING

UNIVERSITI TEKNOLOGI PETRONAS

JANUARY 2020

Determination of Fracture Toughness and Strain Energy Release Rate for Basalt/Epoxy Composites

by

Chandreshah Lal

22770

Dissertation submitted in partial fulfilment of

the requirements for the

Bachelor of Engineering (Hons)

(Mechanical Engineering)

JANUARY 2020

Universiti Teknologi PETRONAS,

32610 Bandar Seri Iskandar,

Perak Darul Ridzuan

CERTIFICATION OF APPROVAL

Determination of Fracture Toughness and Strain Energy Release Rate for Basalt/Epoxy Composites

by

Chandreshah Lal

22770

A project dissertation submitted to the
Mechanical Engineering Programme
Universiti Teknologi PETRONAS
in partial fulfilment of the requirement for the
BACHELOR OF ENGINEERING (Hons)
(MECHANICAL ENGINEERING)

Approved by,

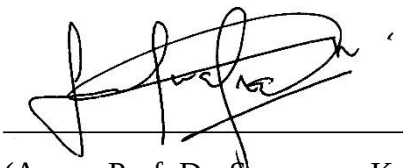

(Assoc. Prof. Dr. Saravanan Karuppanan)

UNIVERSITI TEKNOLOGI PETRONAS
BANDAR SERI ISKANDAR, PERAK
January 2020

CERTIFICATION OF ORIGINALITY

This is to certify that I am responsible for the work submitted in this project, that the original work is my own except as specified in the references and acknowledgements, and that the original work contained herein have not been undertaken or done by unspecified sources or persons.

_____

CHANDRESHAH LAL

ABSTRACT

The consideration of using natural fibres in composites is an attempt to produce sustainable and cost-friendly materials. This study focuses on determining the fracture toughness and strain energy release rate of basalt fibre and epoxy matrix composites. The determination of fracture behaviour will allow for design optimization of components and the experimental values are useful for numerical analysis. Samples tested are unidirectional plies of the basalt fibre which are in 0˚ and 90˚ fibre orientations. This will provide an in depth understanding on the fracture properties of unidirectional samples if they exhibit intralaminar or translaminar fracture behaviour. The experiments are conducted via compact tension and compact compression specimens. The standard testing method utilized was the ASTM D 5045 (Standard test methods for Plane-Strain Fracture Toughness and Strain Energy Release Rate of Plastic Materials) which is compatible for plastic matrices. Compliance calibration technique was used for data analysis and post-test analysis includes analysing the fractured cross section of the specimens with SEM. Experiments conducted showed that the data for unidirectional 0˚ in tension can be determined whereas for unidirectional 90˚, it was difficult and challenging. The values for unidirectional 0˚ were 237.77 kJ/m^2 ± 50.39 for initiation and 15.98 kJ/m^2 ± 0.8 for propagation. Numerical data for compression tests obtained were inaccurate as the fracture had occurred elsewhere rather than at the crack tip. Fibre bridging occurred for the specimens in both tension and compression. Matrix damage was more prominent than fibre damage for the samples and it can be concluded that this was due to the low interface strength and fibre matrix volume ratio.

ACKNOWLEDGEMENTS

Completing this project required tremendous effort and guidance wherein some of the notable contributors include my supervisor Dr. Saravanan Karuppanan, mentor Mr. Zubair Sajid and laboratory technologists.

Dr. Saravanan had always been there to guide me with the project and monitored my progress each week. The weekly discussion helped me to solve and overcome some of the obstacles in my project. I would hereby like to express my gratitude to Dr. Saravanan for taking some time out of his busy schedule to guide me whenever necessary.

Having a mentor like Mr. Zubair meant that at every step of this project, I was well assisted, and I managed to learn more about the subject from him. His knowledge on this subject has led me to solve some of the ambiguities and made it easier to perform experiments with his assistance.

I would also like to express my appreciation towards the laboratory technologists at Universiti Teknologi PETRONAS for assisting with experimentation and usage of equipment. Mr. Johan Ariff and Mr. Danial Abdul Rani had assisted me the experiments and guided me with the utilization of the laboratory. Without their help, it would be difficult to complete this project within the given timeframe.

TABLE OF CONTENTS

LIST OF FIGURES

LIST OF TABLES

CHAPTER 1

INTRODUCTION

1.1 Background

Composites have been utilized in multiple industries to produce parts as an alternative to using metals or polymers. In addition to matching the mechanical properties of metals, composites are also able to provide superior advantage in terms of being lightweight and corrosion resistance.

In recent development, a pairing of natural fibres and epoxies have given a wide range of options and possibilities to produce composite structures. This study focuses on the composite structures which are produced with basalt/epoxy composites. Considering that this combination is relatively novel, certain properties of this composite has yet to be determined. This information will provide the data required for application purposes and the characteristics of the composite.

In this study, the focus is on unidirectional laminates produced with basalt fibres and epoxy resin. Laminates are structures made up of multiple plies of fibres which are arranged in specific orientations and reinforced with a polymer matrix. The fibre orientations within the ply affects the load bearing capability of the composite structure. The utilization of unidirectional fibre plies allows for maximum tensile load bearing capability when the loading direction is parallel to the fibre direction.

An important property for composites which is necessary to be studied is the ability of the material to resist crack initiation and propagation. It is also known as fracture toughness. Understanding the behaviour of the composite and its response towards fracture allows for optimization for the usage of the composite. The amount of energy which is lost when the structure fails will provide information on the load bearing capability of the composite. The manufacturing defects of these composite structures namely delamination and voids will be the catalyst towards failure upon usage. This is due to the amplification of stress concentration at the defects that eventually leads to crack initiation followed by the propagation.

The propagation of the crack highly depends on the direction of loading subjected to the composite. The classification of the cracks according to the direction of propagation are listed as below and demonstrated in Figure 1.1:

- Interlaminar cracks: Cracks which propagate between the fibre plies
- Intralaminar cracks: Cracks which propagate within the fibre ply
- Translaminar cracks: Cracks which propagate along the cross section of the fibres

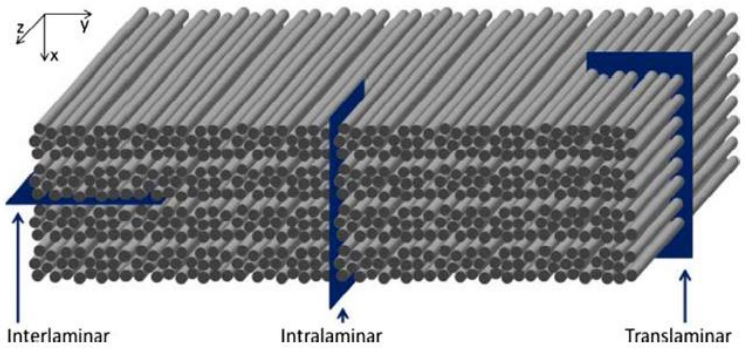

Figure 1.1: Directions and the classification of cracks [1]

Due to the different directions of crack propagation, it is necessary to understand and determine the fracture toughness of the composite in all directions. Therefore, the study of intralaminar and translaminar fracture behaviour is necessary. The unidirectional fibre orientations which will be studied are in 0˚ and 90˚. The type

of loading (tension or compression) would also affect the cracking behaviour of the composite and it is a necessary parameter to be considered as well.

Fracture toughness and energy release rate are necessary properties as design considerations and safety factors are highly dependent on the ability of the material to sustain and respond to the load during failure.

1.2 Problem Statement

In accordance with the 3 types of crack propagations discussed earlier, each mode provides different information about the materials' fracture toughness behaviour. According to Pinho et al. [2] material characterization is necessary for consideration and application in numerical analysis and simulation. For the purpose of design, the orientation of the fibres and their respective fracture behaviour can be used to optimize the design according to the usage of the component and load application. To develop accurate finite element models, material properties such as fracture energy should be well known. This highlights the importance of determining the intralaminar and translaminar fracture toughness for unidirectional samples of the basalt/epoxy composites which are still unavailable.

1.3 Objectives

The objectives of this project are to:

a) Determine the fracture toughness (K_{IC}) and strain energy release rate (G_{IC}) of basalt/epoxy laminates in tensile and compression modes.
b) Evaluate the damage at microscopic level in basalt/epoxy laminates and characterize the fracture.

1.4 Scope of Study

The scope of this study is constrained to the determination of the strain energy release rate and the fracture behaviour. The study will be conducted experimentally using compact tension and compact compression specimens. The specimens will be loaded in tension and compression to understand the crack propagation behaviour.

The study will focus on 2 orientations of unidirectional fibre laminates (0˚ and 90˚) shown in Figure 1.2. The experimental outcome will provide data on the mechanical properties of the basalt/epoxy composite material and characterize the cracks as either intralaminar or translaminar.

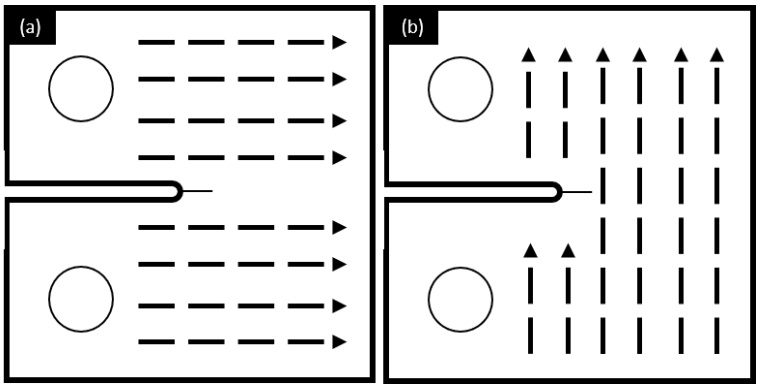

Figure 1.2: Fibre orientations of (a) unidirectional 0˚ (b) unidirectional 90˚

CHAPTER 2

LITERATURE REVIEW

2.1 Fracture Mechanics of Composite and Quantification

For this study, the necessary aspect which is required for examination is the intralaminar and translaminar fracture toughness of basalt/epoxy composite laminates. The fracture toughness is known as the crack resistance of a material, so the data would be derived from the cracking behaviour of the material. The crack resistance is divided into two phenomenon which are crack initiation and crack propagation. Each of these phenomena will demonstrate the response of the material corresponding to the application of load.

The stress intensity factor, K is a necessary parameter which is used to represent the stress at the crack tip. The critical stress which causes the crack to initiate and to propagate is denoted as K_{IC}. The subscript C represents critical and I is for the mode of loading which is in tension.

Strain energy release rate, G is used to quantify the amount of energy loss per unit area of crack growth. The critical value for this parameter is represented as G_{IC}. This parameter is particularly important for plastic matrices as the rate of energy loss corresponds to the damage resistance of the matrix. The correlation between the energy release rate and the length of the crack can be observed with a graph known as R-curve to better understand the crack resistance behaviour which is shown in Figure 2.1.

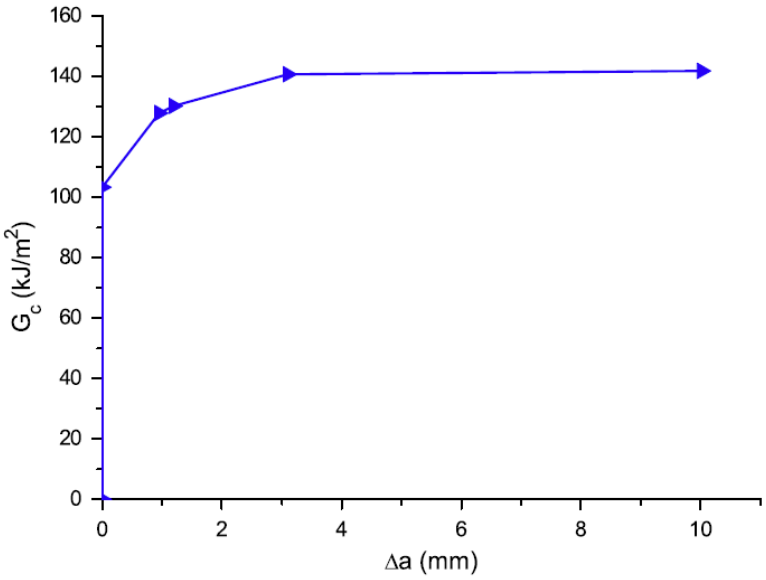

Figure 2.1: Graph of crack resistance [5]

Some factors which are important to study include the presence of surface and internal cracks on the material. These imperfections will cause the failure to begin at a much lower condition than the applied stress. With the presence of defects, the stress intensity in proximity to the crack tip is amplified due to zero area which had been described in [6].

According to ASTM D5045 [4] which is used for determining the fracture toughness and energy release rate of polymers, the material can be assumed to comply with the concept of Linear Elastic Fracture Mechanics (LEFM) as the matrix being used is epoxy and is known to be brittle. Chabchoub et al. [7] stated that LEFM is usually considered for elastic brittle composite materials whereas Elastic Plastic Fracture Mechanics (EPFM) is commonly used for ductile composite materials. For LEFM, the important parameters include critical stress intensity factor, critical strain energy release rate and the R-curve. These coincide with the data obtained in [8, 9] as they have utilized the same concept due to their matrix being epoxies.

2.2 Testing Procedures Identification

There are 2 geometries of sample which can be utilized to determine the fracture toughness for the tensile loading. The first would be to utilize the compact

tension (CT) specimen shown in Figure 2.2. and the second is a single edge notch bend (SENB) or (3-point bending) test shown in Figure 2.3. These test methods have been utilized by Khan et al. [9] and recommended by Prasad et al. [6].

CT specimens are designed for instances where the crack growth conditions are stable for determining the fracture toughness [10]. Making sure that the stability of the crack growth is maintained, the testing parameters should be selected so that the crack propagation is stable throughout the test. One of the factors to control the propagation would be adjusting the crosshead speed to a reasonable amount. The recommended range is within 0.5 mm/min to 1 mm/min.

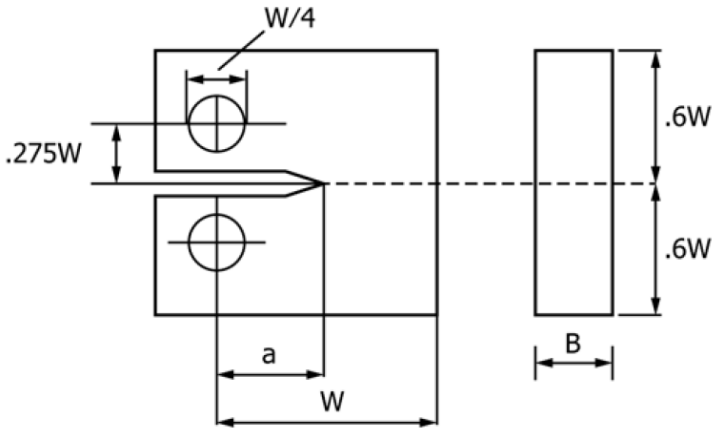

Figure 2.2: Compact Tension (CT) [5]

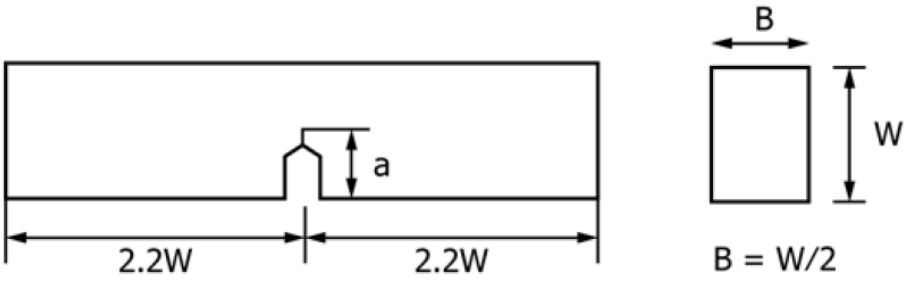

Figure 2.3: Single Edge Notch Bend (SENB) [5]

Currently, there is no specific standard available to determine fracture toughness for complex damage phenomenon such as compressive fibre failure which induces a lot of secondary damages types. Therefore, the compact tension specimen

had been modified to be loaded in compression for the study conducted by Pinho et al. and Lisle et al. in [2, 11]. The sample for the compact compression had been wedged cut and can be observed in Figure 2.4 which had been used by Pinho et al. [2]. The idea behind this is to avoid the edges from colliding when being compressed. In situations where it is not wedged cut, the compression will discontinue, and the test would not be complete.

An alternative for the compression test using CC specimen is to conduct a 4-point bending test with a SENB specimen. This method is effective to provide the fracture toughness in compressive mode and had been utilized by Laffan et al. [3]. A recommendation for compression loading of CC specimen is provided by ASTM D5045 [4] whereby the specimen is required to be loaded to 70% of the yield strength in tensile mode of the specimen.

The ASTM E399 Standard used for Fracture toughness of metals is not applicable as the equation for the fracture does not consider the correction factor. This had been proven by Pinho et al. [2] who used similar geometry and without the correction factor, and found the results had discrepancies. The ASTM D5045 [4] uses a similar geometry of the specimen for the test but with optimized correction factor specifically for polymer matrices and is proven to be reliable based on the results obtained by Khan et al. [9].

2.3 Variation in Data Acquisition Techniques

2.3.1 Digital Image Correlation (DIC)

This technique is used to quantify the displacement of the surface for the samples. Speckle patterns are made on the surface of the specimen and images are taken across a certain time step. The shifting location of the patterns on the surface throughout the experiment can be then analysed. The displacement of the pattern provides information on the crack propagation and its direction. This method had been used in [2, 12, 13] and is capable of providing sufficient information to understand the fracture behaviour.

2.3.2 Linear Variable Displacement Transducer (LVDT)

This apparatus has been used in [1, 5, 13] to obtain the displacement of the specimen. When the load is applied, the specimen moves, and the displacement is recorded. This data can then be used to get the modulus of elasticity which is used for further calculations to obtain the strain energy release rate.

2.3.3 Infrared Thermography

Lisle et al. [11] have utilized infrared thermography to determine fracture toughness and crack behaviour by studying the fracture locally. The heat generated from the damage will be picked up with the infrared cameras and which provide details on the fracture behaviour of the specimen. The two phenomenon which occurs for compression loaded specimen are kink band and crushing. These have to be separated in order to obtain accurate values. Applying a localized approach for analysis will yield accurate results, although there is a debate on this technique to obtain the strain energy release rate of the material. This is due to some assumptions being made based on the regions of the heat fluctuations produced as the material fractures.

2.3.4 Visual Crack Observation

This method is used to quantify the crack growth visually using digital cameras and had been utilized by Frossard et al. and Liu et al. [1, 8]. There is a possibility to obtain discrepancies using this technique as the correspondence of the visual observation with the actual crack length may vary. The assumption is that the visual crack growth is similar to the crack within the specimen. A video recording of the experiment will be taken to observe the crack growth of the sample. The resistance curve (R-curve) is plotted with the energy release rate and visually observed crack growth which gives information on the crack resistance behaviour.

2.3.5 Acoustic Emission

The acoustic emission is one of the most useful methods of data acquisition as this technique is able to record the soundwaves which are emitted during the test. It provides information on the internal crack propagation and provides better accuracy for crack measurement when compared to the visual observation. This aids in identification of the extent of actual crack propagation. This method had been applied by Laffan et al. [3] for the determination of fracture toughness in compression loading and the position of the sensor are demonstrated in Figure 2.4.

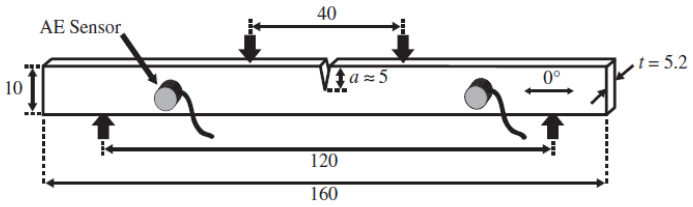

Figure 2.4: Specimen with Acoustic Emission Sensors [3]

2.3.6 Conclusion

Among these acquisition techniques, the most recommended would be the digital image correlation and acoustic emission. They have a much higher accuracy and the results would have minimal discrepancies. As for the others, they provide a more conventional approach and have some possibility of error but nevertheless have been used by other authors to obtain useful experimental values with the right data treatment.

2.4 Post Experimental Analysis

Analysis of the damage can be done using ultrasound scan (C-scan) which has been utilized by Pinho et al. and Liu et al. [2, 8]. The result obtained shows that the overall damage zone is large in compression mode when compared to tension mode, which justifies the presence of the secondary damages. Figure 2.5 shows the damaged region between the two loading modes. The fibre kinking and crushing have resulted in a larger damage region for the compressively loaded specimen.

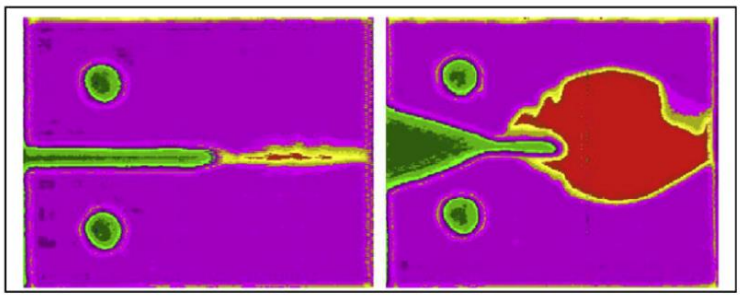

Figure 2.5: C-Scan of the specimen in tension (left) and compression (right) [2]

Scanning electron microscopy (SEM) can be utilized to view the damage of the fractured region. The fibre breakage and the matrix cracking can be observed to understand the propagation of the cracks. This method is ideal to understand the fracture behaviour on the composite as matrix and fibres can be analysed at a microscopic level. Figure 2.6 shows a sample of the damaged cross section being analysed using this technique.

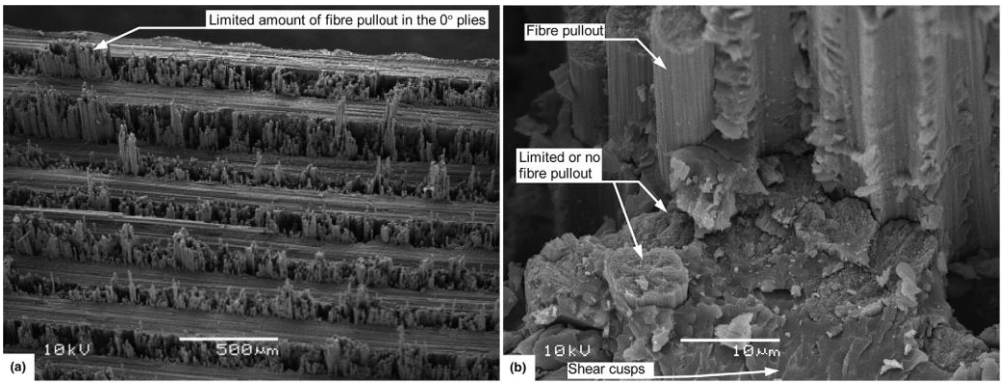

Figure 2.6: Sample of damaged sections viewed with SEM [2]

2.5 Behaviour of Material Under Tensile Load

From the tests conducted, Liu et al. [8] noticed that the specimens tend to experience out of plane displacement, and this potentially affects the data. Structural supports are to be fitted across the composite plate to hold it in place. When the specimen is subjected to the tensile loading, there is a possibility to flex or curve which will compromise the boundary conditions set for the experiment.

The additional fixtures should provide support to the specimen while maintaining the boundary conditions. It should not induce additional stress which may compromise structural rigidity of the composite specimen. The experiment done by Liu et al. [8], utilized a finite element model to identify the weak points during the testing which is demonstrated in Figure 2.7 and they have designed the fixtures shown in Figure 2.8 accordingly to prevent deflection and maintain the boundary conditions.

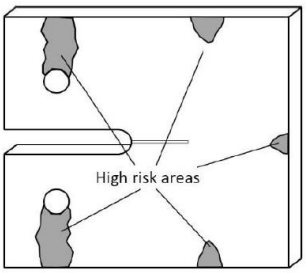

Figure 2.7: High risk areas. [8]

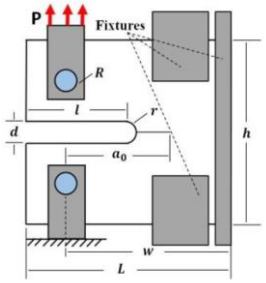

Figure 2.8: Fixtures designed to prevent deflection. [8]

2.6 Compressive Failure of Notched Specimen

The data obtained from Pinho et al. [2] showed that the initiation values are possible to be determined, however due to the damage comprising of crushing and also the kink band formation, the complex damage is difficult to be analysed and the

propagation values for the crack are unable to be determined. In comparison with the work by Soutis et al. [14], the failure occurred by crack which had propagated parallel to the fibres and no meaningful data was obtained.

The compressive failure for longitudinal fibre has also been studied by Laffan et al. [3]. They have resorted with the elimination of 0˚ plies from the unidirectional specimens and used 4-point bending test in an attempt to prevent the intralaminar splitting. The damage was observed to be initiated with 45˚ angle and proceeds with a mode 1 crack which then forms a single in-plane kink band that extends deeper into the test specimen.

Therefore, with the two orientations of unidirectional fibres being tested, the data obtained may be useful in one of the orientations. This will have to be tested experimentally to compare and characterize the behaviour. Besides, with the improvement of structural rigidity with the fixtures to support the specimen through the test, the damages are expected to be more controlled and useful experimental values may be determined.

2.7 Effect of Fibre Orientation

In theory, with 2 different orientations of the unidirectional fibres, the tensile loading will result in a varying profile of the crack propagation along the affected region which has a high concentration of stress. The crack propagates in different directions and therefore can be classified as either intralaminar or translaminar. This consideration will ensure that the data obtained is accurate for the required loading application.

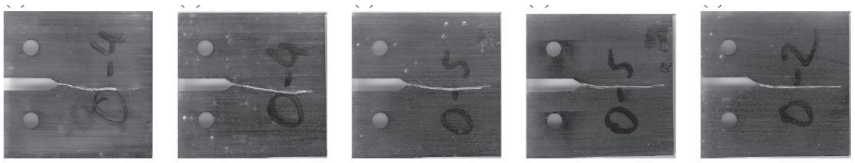

Figure 2.9: Crack paths in CT specimen for 0˚ direction [15]

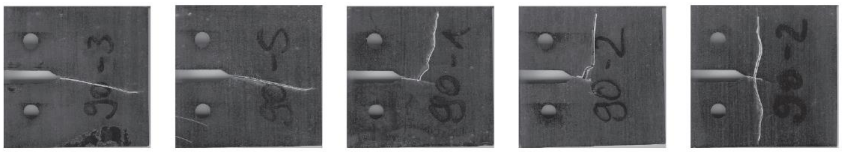

Figure 2.10: Crack paths in CT specimen for 90˚ direction. [15]

This is proven in the study conducted by Keck and Fulland [15] who have conducted the test with different fibre volume fractions and fibre orientations as shown in Figure 2.9 and Figure 2.10. The direction of propagation is largely dependent on the fibre volume fraction of the composite specimen.

Therefore, to well understand the crack propagation behaviour between the two unidirectional orientations, the tests in tension would be necessary in which the consistency in the trajectory of the crack propagation could also be determined.

CHAPTER 3

METHODOLOGY

3.1 Sample Preparation

The determination of the composites fracture toughness properties can be done based on ASTM D 5045 – Standard Test Methods for Plane-Strain Fracture Toughness and Strain Energy Release Rate of Plastic Materials [4]. This standard is applicable and had been used by Khan et al. [9]. Considering that the damages will propagate within the plastic matrix (epoxy), this standard is acceptable to be utilized for experimentation. Specimens for this experiment were manufactured using Vacuum Infusion Process (VIP) as it helps with maintaining a higher fibre to resin volume ratio. With lesser resin, the mass of the specimen is also reduced which is an advantage.

The specimens selected are the compact tension specimens. The notch was made by filing the centre of the specimen. This method was used to prevent inducing damage to the plies. The pre-crack was induced by carving a thin 10 mm long crack at the edge of the notch using a sharp razor of width not more than 0.5 mm.

The dimensions of the specimen made were according to the illustration in Figure 3.1 which was developed by Keck and Fulland [15] by referring to the guideline in the standard [4]. The dimensions are in millimetres. The specimens made have thicknesses of 4 mm - 4.5 mm.

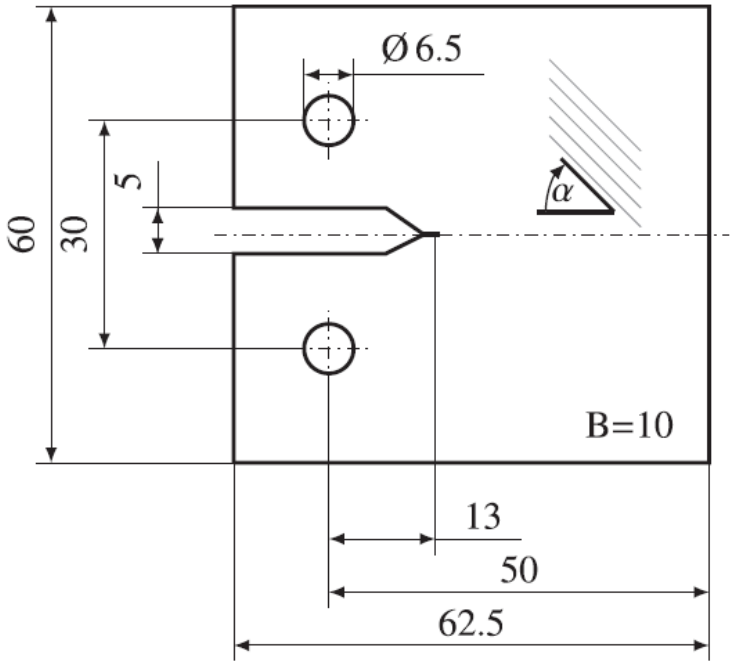

Figure 3.1: Dimensions of specimen with unit in millimetres (mm) [15]

For the compact compression test on the other hand, similar specimen geometry can be used. Some minor changes must be made due to the nature of the test. As compression occurs, the two edges collide and can be prevented by cutting a wedge from the edge to the centre of the notch. It had been utilized by Pinho et al. [2] to conduct the compact compression test. Figure 3.2 shows an example of the specimen with the dashed lines representing the region which should be trimmed.

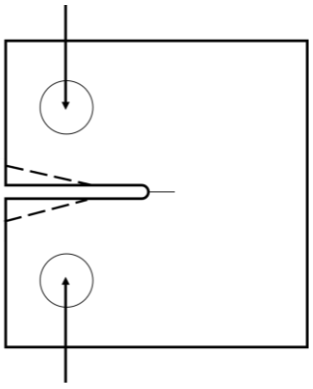

Figure 3.2: Compact compression (CC) specimen

3.2 Measurement Techniques

Measurement instruments that have been proposed for utilization are listed below and had been used for testing depending on their availability in Universiti Teknologi PETRONAS.

3.2.1 Linear Variable Displacement Transducer (LVDT)

The LVDT is used to measure the linear displacement. The clevis for the sample has an extended arm which can be used as a reference surface. The vertical displacement of the LVDT due to the crack opening and propagation will provide data for the applied load against the displacement measured.

3.2.2 Visual Crack Observation

This is done using digital cameras which are placed in front of the specimen during the test. Pictures are taken during intervals to capture the propagation of the crack visually. For better analysis, the section which the crack is estimated to propagate is painted in white and scaled for better contrasting as shown in Figure 3.3.

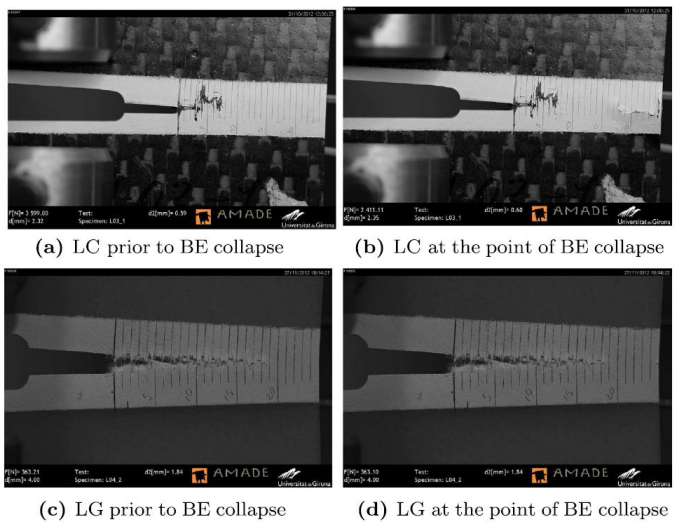

(a) LC prior to BE collapse (b) LC at the point of BE collapse

(c) LG prior to BE collapse (d) LG at the point of BE collapse

Figure 3.3: Painted surface on specimen for visual crack measurement [10]

3.3 Calculations and Analysis

The equations for the calculations have been obtained from the ASTM D5045 [4] testing standard and have been listed accordingly as Equation 1 and 2. The calculation of K_Q is necessary as it represents the estimated stress intensity factor value. This will serve as a reference to determine the accuracy of the experimental results.

$$K_Q = \left(\frac{P_Q}{B\sqrt{W}} \right) f(x) \tag{1}$$

where (0 < x < 1):

$$f(x) = 6x^{1/2} \frac{[1.99 - x(1-x)(2.15 - 3.93x) + 2.7x^2)]}{(1+2x)(1-x)^{3/2}} \tag{2}$$

where K_Q is the estimated Stress Intensity Factor in MPa.m$^{1/2}$
P = Applied load in kN, B = Specimen thickness in cm
W = Specimen width in cm, a = crack length in cm, X= a/W
$f(x)$ = calibration factor

The plain strain fracture toughness (K_{IC}) can be determined using equation 1 with a modified calibration factor shown in Equation 3 and critical strain energy release rate (G_{IC}) can be computed using Equation 4.

$$f(x) = \frac{(2+x)(0.886 + 4.64x - 13.32x^2 + 14.72x^3 - 5.6x^4)}{(1-x)^{3/2}} \tag{3}$$

$$G_{IC} = \frac{\left(1-\nu^2\right)\left(K_{IC}\right)^2}{E} \tag{4}$$

.

where G_{IC} is the Critical Strain Energy Release Rate in kJ/m^2
ν = Poisson's Ratio, E = Elastic Modulus

3.4 Data Reduction

Besides using the equations, data reduction was performed to get the values using the two techniques listed below. These techniques allow direct computation for the critical strain energy release rate. The comparison between the results from these two methods would provide more accurate values after analysing the difference.

3.4.1 Compliance Calibration Method

This method utilizes the compliance obtained from the load displacement graphs from the experiments and correlates the data with the visual crack length obtained from the digital cameras. The critical strain energy release rate will be obtained by calculating the change in compliance, *C* and the crack length. Figure 3.4 shows the method to determine the compliance from the load displacement curve.

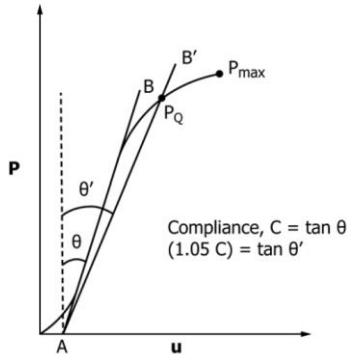

Figure 3.4: Load displacement curve for compliance [16]

$$G_{IC} = \frac{(P_C)^2}{2t}\frac{dC}{da} \tag{5}$$

$$C = \tan\theta \tag{6}$$

Equation 5 shows the method to calculate the critical strain energy release rate with the change in compliance and Equation 6 can be used to calculate the compliance.

3.4.2 Area Method

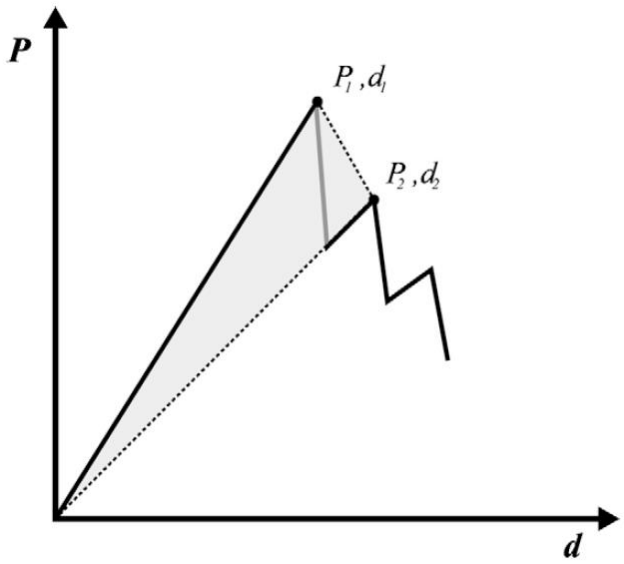

Figure 3.5: Load displacement curve with shaded area [16]

$$G_{IC} = \frac{1}{2t_{\Delta}a}\left(P_1D_2 - P_2D_1\right) \tag{7}$$

The energy released during the fracture is compared. The peak load is compared with the second peak after the drop as demonstrated in Figure 3.5. The area within the shaded region represents the energy consumed for crack growth. Critical strain energy release rate can be obtained using by Equation 7 obtained in [16].

3.5 Experimental Planning

Table 3.1: List of samples

Experiment	Orientation	
	0°	90°
Compact Tension (CT)	CT-0-1	CT-90-1
	CT-0-2	CT-90-2
	CT-0-3	CT-90-3
Compact Compression (CC)	CC-0-1	CC-90-1
	CC-0-2	CC-90-2
	CC-0-3	CC-90-3

With reference to Table 3.1, the experiments will be conducted as planned. The minimum required samples for composite testing are three. 12 samples will be used for the testing. Extra samples have been made considering the probability of the experiment to fail and preliminary testing.

3.6 List of Equipment

3.6.1 Universal Testing Machine (5 kN)

This machine was used to conduct the test in tension and compression. Some additional fixtures such as clevis was prepared to compensate for the geometry of the specimen and the loading conditions of the machine. The crosshead speed selected for the experiment was set at 0.5 mm/min for both tension and compression. The slow crosshead speed was selected to aid visual crack observation and maintain stable crack growth. This apparatus is available in Block 17, Universiti Teknologi PETRONAS and LVDT was attached to the hydraulics arm of the machine to measure the displacement.

3.6.2 Scanning Electron Microscopy (SEM)

Scanning electron microscopy (SEM) will be used to view the microstructure of the damaged regions, namely the notched and cracked regions. The images from the scans will display the damage profile of the fibre and matrix. By interpreting the images, the study on the crack initiation and propagation behaviour will be possible. The extent of damage experienced by the fibre and matrix can also be viewed and with the profile, the experimental results will be well justified.

3.6.3 Optical Microscope

The optical microscope will be used to view the notch and the crack tip. It is necessary to have a small and sharp crack tip to ensure high stress intensity. This aids with controlling the direction of crack growth. Upon creating the notch, the crack tip will be cut using a razor blade and the size of the tip will be observed to ensure consistency and symmetry.

3.7 Project Plan

To monitor the progress and plan the duration for key activities, a project Gantt Chart has been developed as shown in Figure 3.6.

No	Tasks	Duration (Week)													
		1	2	3	4	5	6	7	8	9	10	11	12	13	14
1	Literature Review														
2	Manufacturing Samples														
3	Testing														
4	Experimentation														

No	Tasks	Duration (Week)													
		15	16	17	18	19	20	21	22	23	24	25	26	27	28
4	Experimentation														
5	Post Testing Analysis														
6	Report Preparation														
7	Amendments & Submission														

Figure 3.6: Overall Project Gantt Chart

3.8 Key Milestones

The key milestones are used to gauge the progress for this project up till the completion as shown in Figure 3.7.

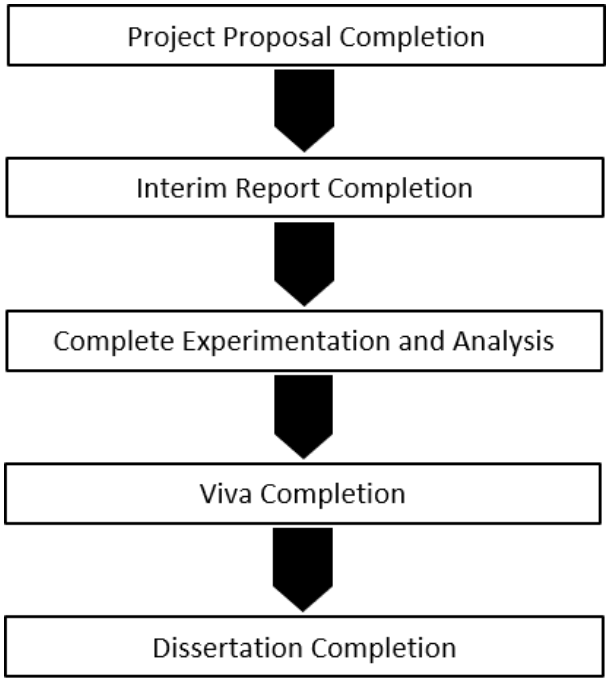

Figure 3.7: Key milestones of the project

CHAPTER 4

RESULTS AND DISCUSSION

4.1 Tensile Tests

4.1.1 Tensile Test of Unidirectional 0˚ Samples

The tensile tests for the unidirectional 0˚ samples were proven to be successful as the boundary conditions were maintained during the test. There was no visible deflection or crack in an undesired location. This shows that the effectiveness of the fixtures played an important role in obtaining meaningful data. The load versus displacement graph have been obtained as shown in Figure 4.1.

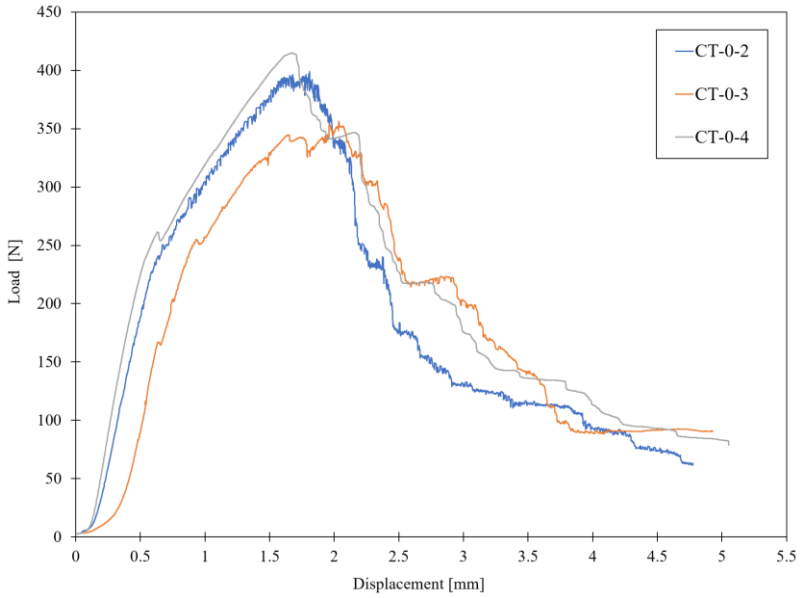

Figure 4.1: Load vs Displacement graph of unidirectional 0˚ samples

The behaviour shows an elastic region at the beginning of the curve. The initial load drop is associated with the initiation of matrix cracking where the load averages at 255.61 N ± 5.37. At the peak it is assumed that the crack begins to propagate as it exceeds the yield strength of the matrix.

Corresponding with the data, the compliance calibration method was applied as it was simpler to compute and obtain the data shown in Figure 4.2. The area method was not used since locating the drops after the peak is difficult from the plot.

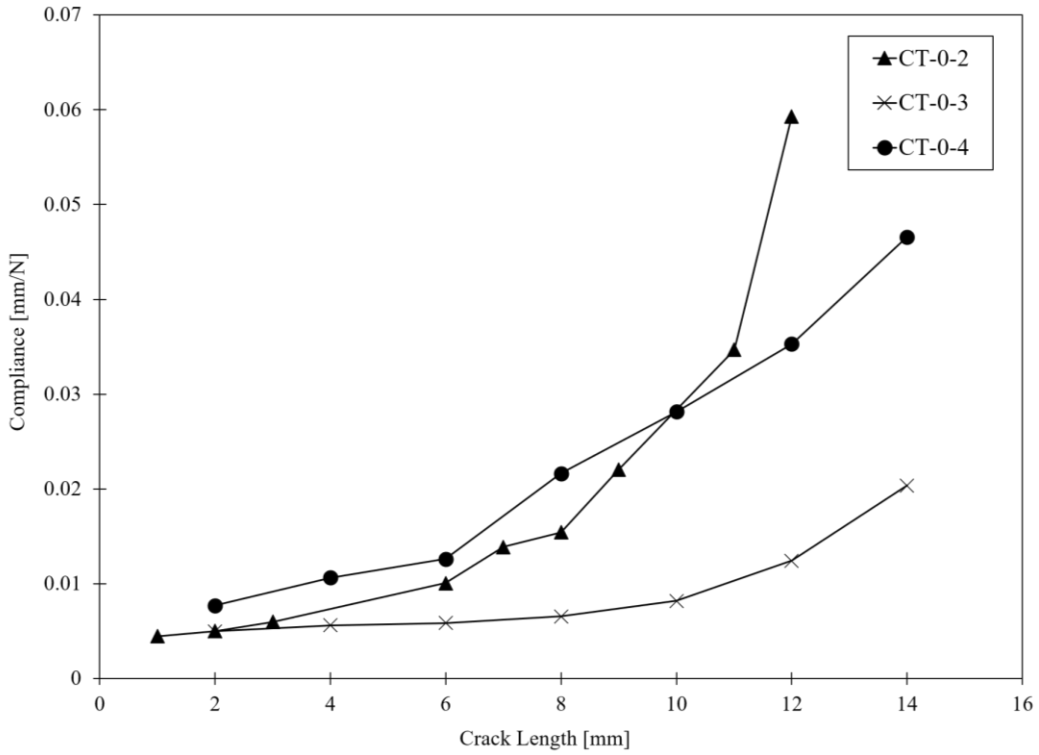

Figure 4.2: Compliance graph of unidirectional 0˚ samples

The strain energy release rate was obtained by plotting the energy against the visual crack propagation which then provides the resistance curve as shown in Figure 4.3. The data shows that the initiation energy is high, and as the crack propagates further, the energy reduces which shows that the fracture toughness is relatively low as the crack extends and reaches a plateau towards 14 mm.

Table 4.1 displays the energy values obtained from the data. Initiation energy was calculated from the point of the first load drop. Propagation energy was calculated by taking the average of the total energies from each point. The average initiation

value obtained was 237.768 kJ/m^2 ± 50.39 and for the propagation, the value was 15.977 kJ/m^2 ± 0.8. The fracture toughness was obtained as well and plotted against the crack length at each point as shown in Figure 4.4.

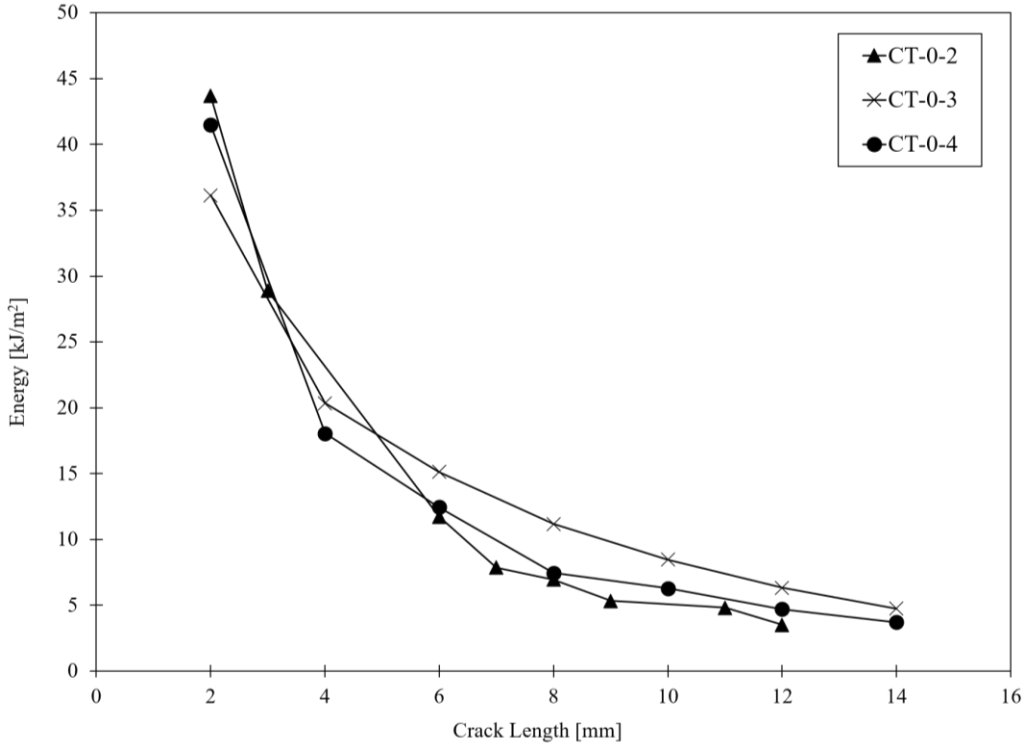

Figure 4.3: Resistance curve of unidirectional 0˚ samples

Table 4.1: Data for unidirectional 0˚ samples

Sample	Initiation Energy (kJ/m^2)	Propagation Energy (kJ/m^2)
CT-0-2	211.097	16.593
CT-0-3	295.891	16.264
CT-0-4	206.316	15.073
Average Value	237.768 ± 50.39	15.977 ± 0.8

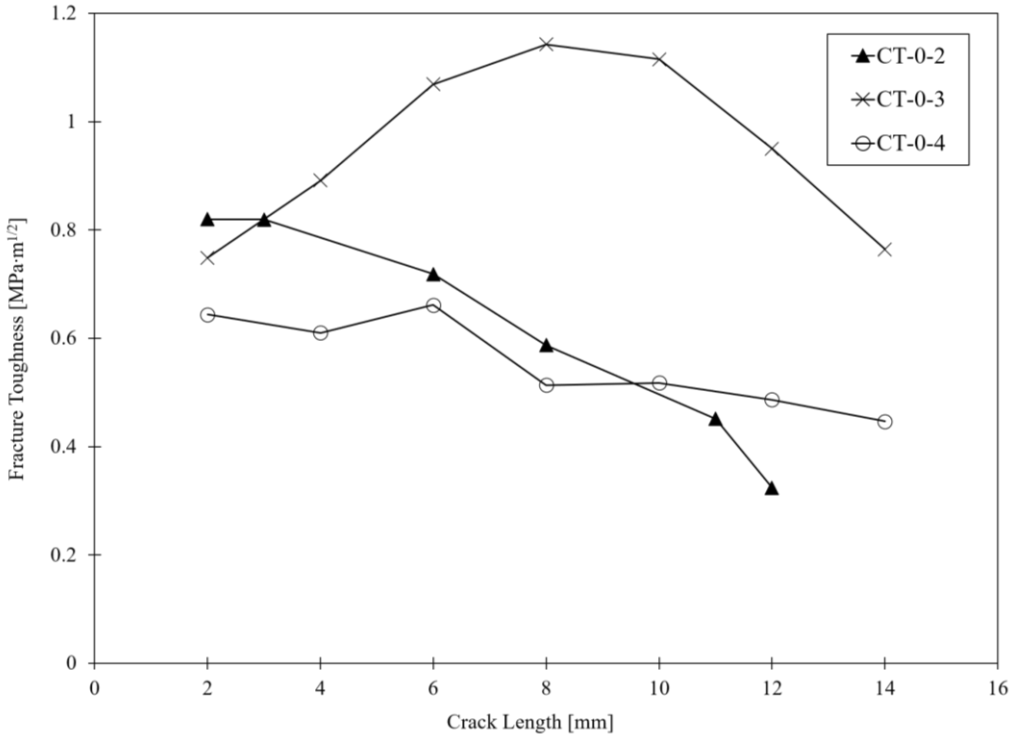

Figure 4.4: Fracture toughness vs crack length for unidirectional 0˚ samples

Visual observation during testing indicated the effect of fibre bridging as the crack tip opening was increased as shown in Figure 4.5 (b). Matrix cracking was observed first followed by the fibre matrix interface failure. Characterizing the crack length visually proved to be a challenge since the separation was not clean and obstructed by the fiber bridging.

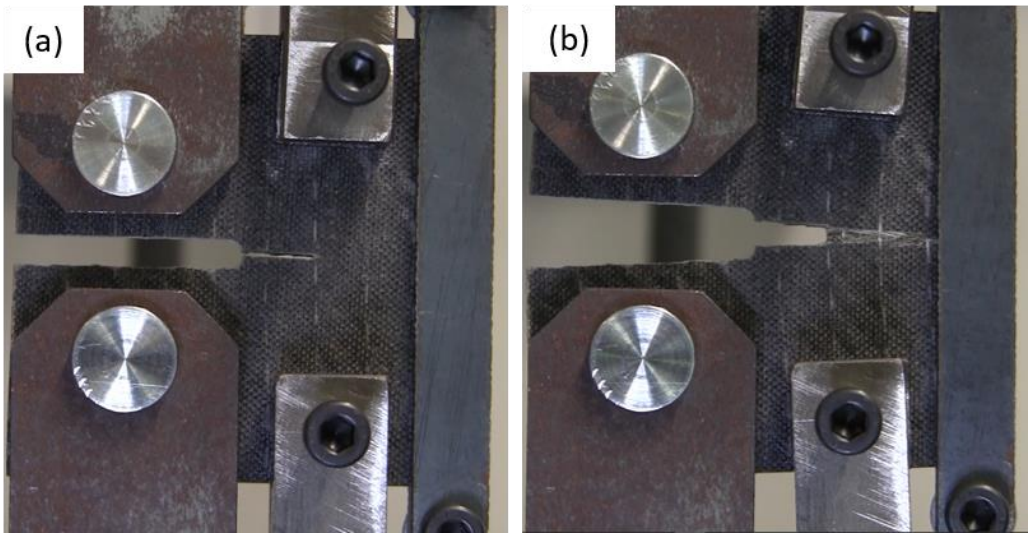

Figure 4.5: Tension (a) before (b) after for unidirectional 0˚ sample

The results from the SEM micrography displayed in Figure 4.6 shows that the fracture is dominant on the matrix and involves the fibre matrix interface failure. It is coherent with the damage observed visually during testing. This is further proven by the phenomenon of fibre debonding from the matrix. This phenomenon coincides with the established hypothesis that the unidirectional 0˚ samples will exhibit intralaminar fracture behaviour when loaded in tension.

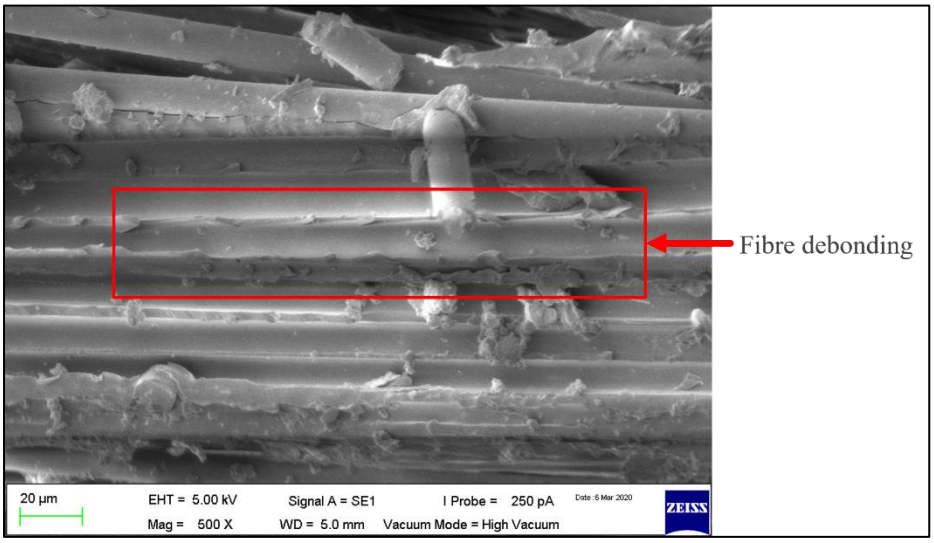

Figure 4.6: SEM micrograph of unidirectional 0˚ sample

4.1.2 Tensile Test of Unidirectional 90˚ Samples

The hypothesis suggested prior to experimentation is that the unidirectional 90˚ samples will experience translaminar fracture behaviour, whereby the crack will propagate along the cross section of the fibres. The strength and load bearing capability obtained was much higher than the unidirectional 0˚ with the load displacement graph shown in Figure 4.7. Visual crack propagation was unable to be conducted since the cracking is not the same for the samples. This is due to the inconsistency of crack propagation direction in either the bottom, top or both sections for each sample tested.

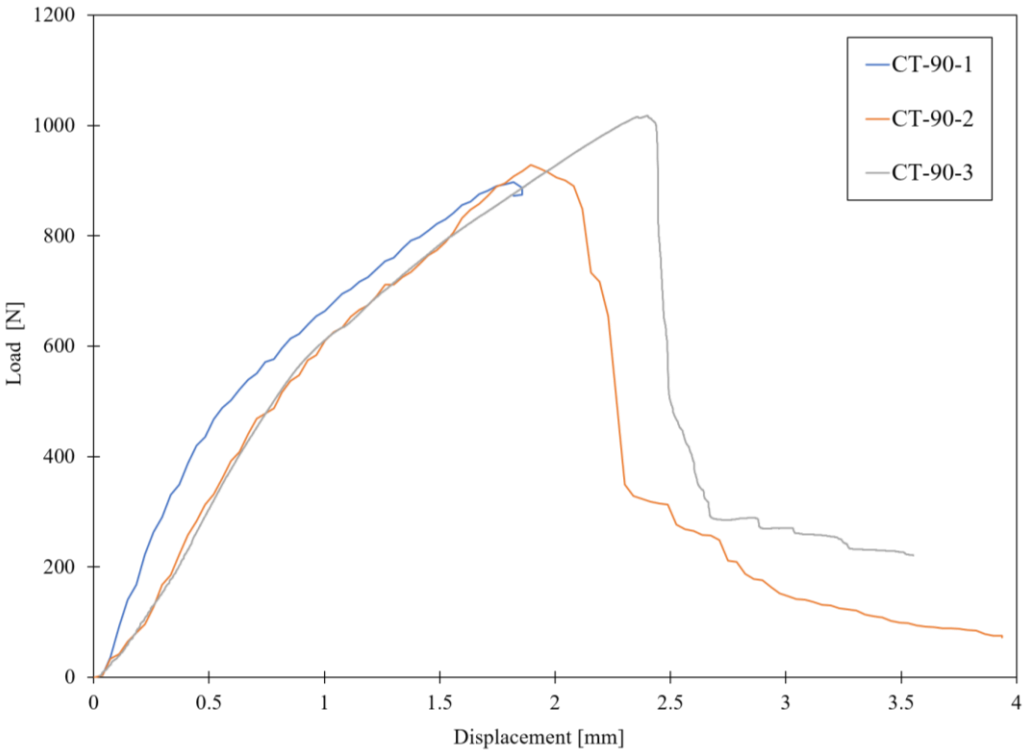

Figure 4.7: Load vs Displacement curve of unidirectional 90˚ samples

The usage of fixtures was deemed to be ineffective for this fibre orientation as crack had initiated at the tip but propagated vertically which was parallel to the fibre direction. Among the three samples tested, this behaviour was inherent. This has led to the conclusion that the poor fibre matrix interface strength caused the matrix to absorb the load rather than distribute it to the fibres. Fibre bridging was observed in Figure 4.8 (b) and it also depicts that the failure is in the fibre direction.

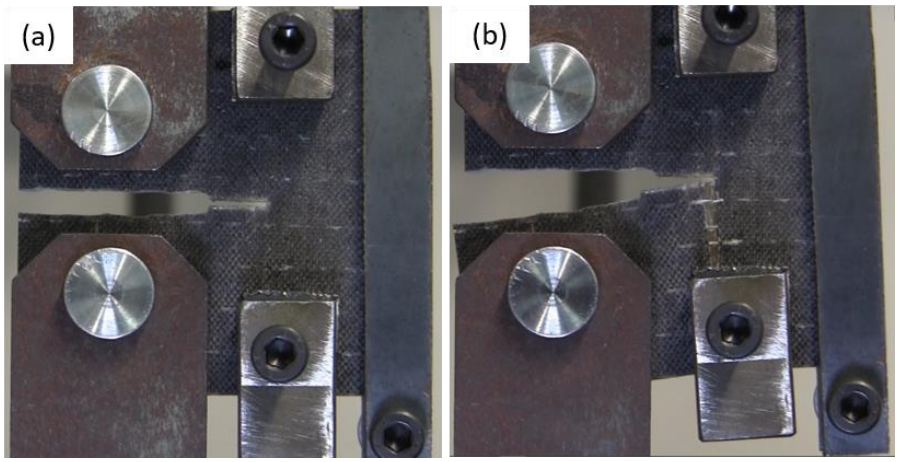

Figure 4.8: Tension (a) before (b) after for unidirectional 90˚ sample

The damage on the unidirectional 90˚ samples are similar to the results obtained by Keck and Fulland [15] who studied the effect of fibre volume fraction on crack propagation path. The fibre volume ratio of 45% for the composite samples is rather high. This also means that there is insufficient matrix to cover the entire surface. This is apparent in the SEM images as the bundles of fibre can be seen with very little matrix coverage as shown in Figure 4.9.

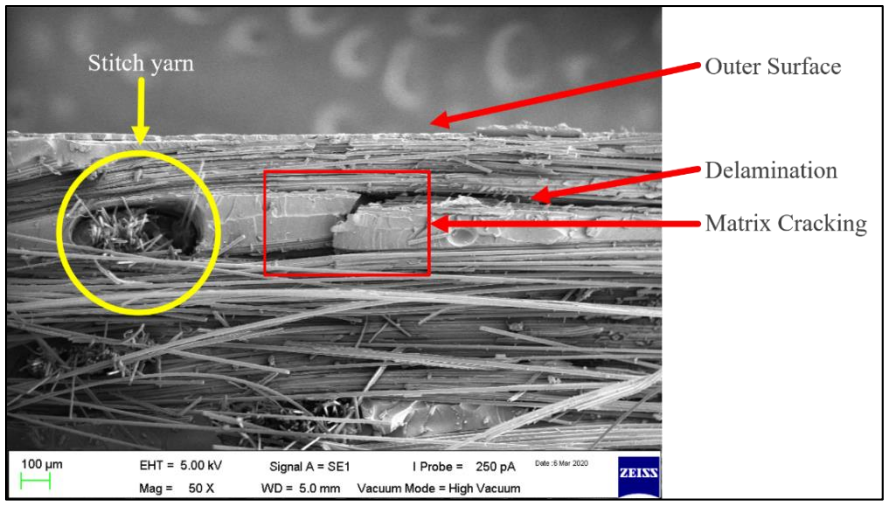

Figure 4.9: SEM image of damaged cross section of unidirectional 90˚ sample

With SEM micrography, cross sectional damage of the fibre was not visible. This shows that most of the fibres did not experience much damage and the failure was dominant on the matrix. Fibre matrix debonding have been observed which is similar to the samples in unidirectional 0˚. This highlights the importance of adhesion properties towards the strength of a composite material.

4.2 Compressive Tests

4.2.1. Compressive Test of Unidirectional 0˚ Samples

The tests conducted in compression were found to be ineffective for the unidirectional 0˚ samples. Despite having a sharp crack tip, the stress concentration was observed to have built up at the edge of the samples as shown in Figure 4.10 (b). This led to a new crack being initiated from the back of the sample as it flared due to the compression. With reference to the three samples tested, the damage mechanism was similar and therefore meaningful data was not possible to be obtained due to the violation of the boundary conditions during the experiment. The geometry of the samples is similar to that of the compact tension with a slight modification to prevent the edges from touching which seemed to be effective. Fibre bridging was observed which indicated fibre debonding from the matrix. Considering the type of damage, which is contrasting with the expected result, an alternative testing for compression properties is proposed to be conducted with a 3 point bending test specimen for the unidirectional 0˚.

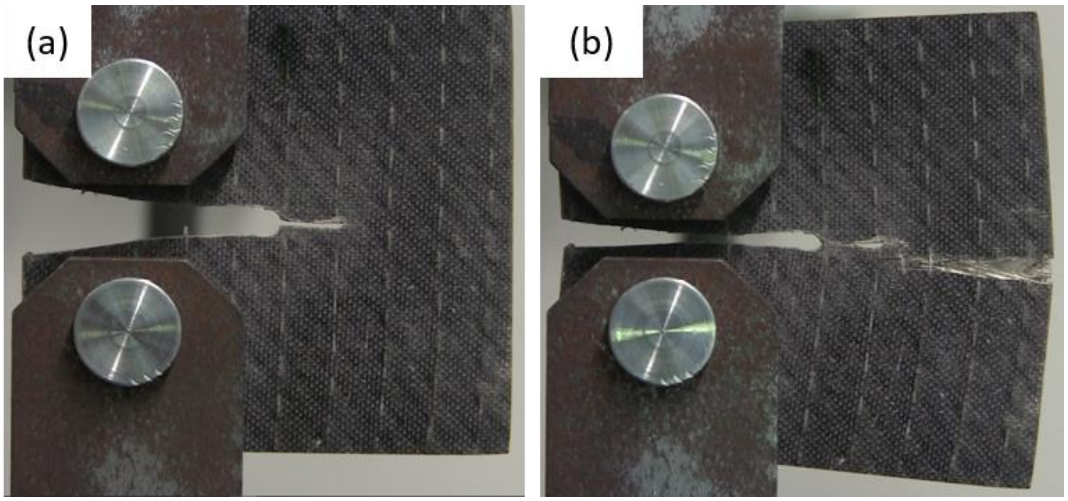

Figure 4.10: Compression (a) before (b) after for unidirectional 0˚ sample

4.2.2. Compressive Test of Unidirectional 90˚ Samples

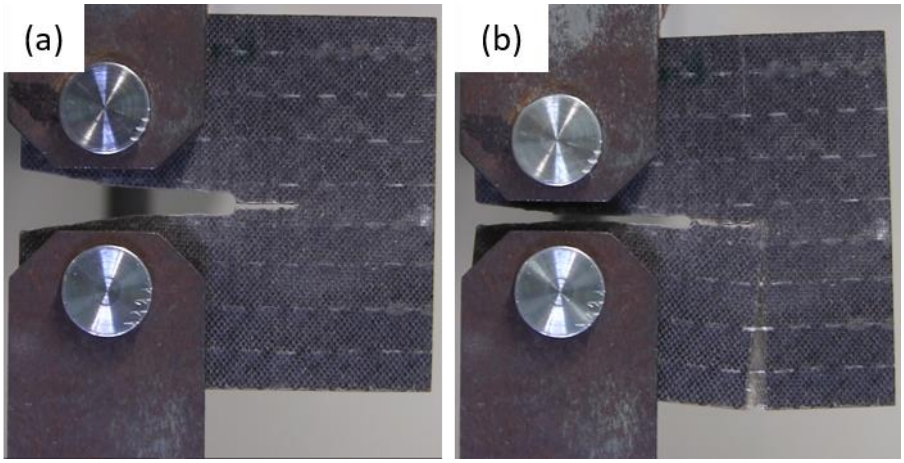

Figure 4.11: Compression (a) before (b) after for unidirectional 90˚ sample

In the case of unidirectional 90˚, the crack was initiated away from the fabricated crack tip as depicted in Figure 4.11 (b). The crack initiated in the similar location to that of the sample in tension. With continuous compression, the sample experienced flaring and the crack propagated to the fabricated crack tip. Numerical results would be invalid in this case since the expected crack initiation location is dissimilar. An alternative testing for compression properties is proposed to be conducted with a 4 point bending test specimen for the unidirectional 90˚.

4.2.3 SEM Micrography

Visual analysis had been conducted via SEM micrography on the cross section of the damaged area. The images reveal that in both cases, the matrix failure was the most dominant as shown in Figures 4.12 and Figure 4.13. Images may have depiction of broken fibres which had been induced during sample preparation for the microscopy. Kink bands which are a common failure observed in compressive tests were not observed for the unidirectional 90˚ samples. This is observed in Figure 4.13, where the fibres were seen to be well aligned and intact with the matrix.

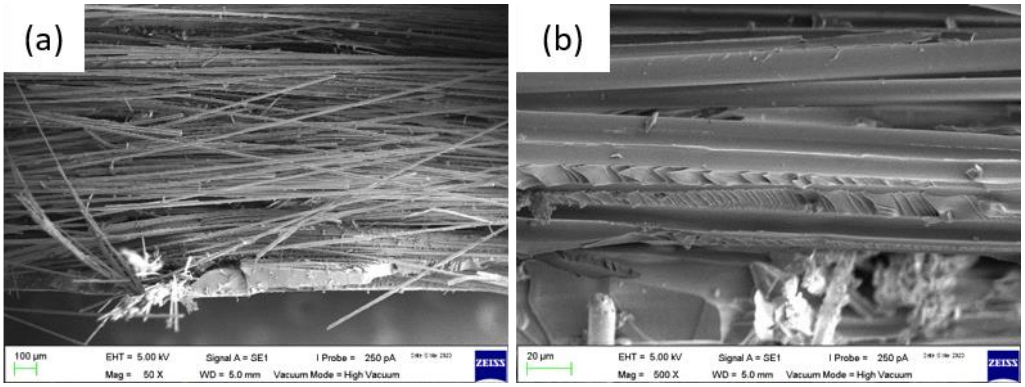

Figure 4.12: (a) Fibre bridging (b) matrix cracking of compressed unidirectional 0˚ sample

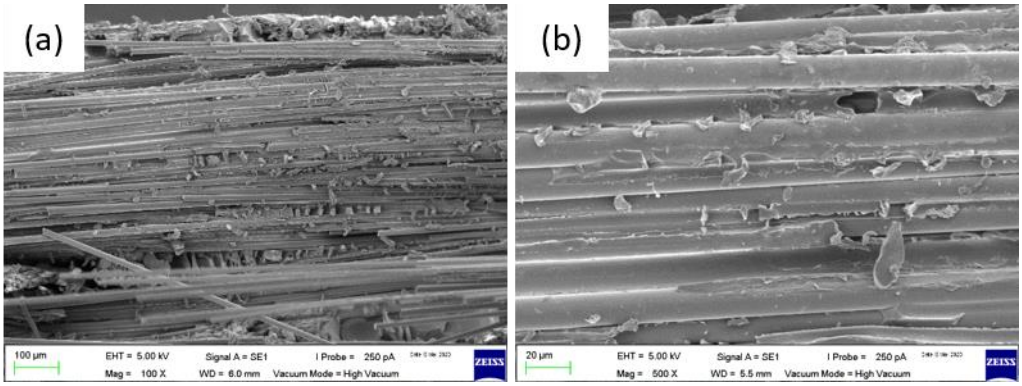

Figure 4.13: Undamaged fibres of compressed unidirectional 90˚ sample

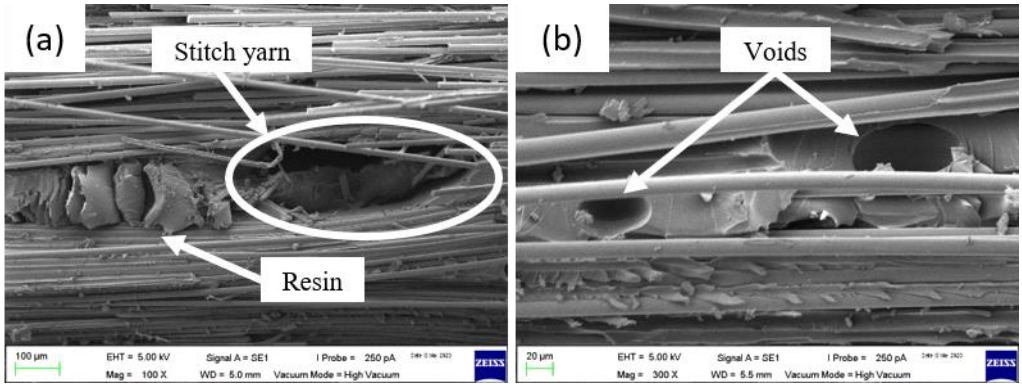

Figure 4.14: (a) Resin build up (b) Voids in the matrix

Further examination of the samples revealed that there was resin build up at the stitch yarn which had caused the flow of resin to halt and compromise the adhesion and coating around the fibres as depicted in Figure 4.14 (a). Voids were also observed in the samples as shown in Figure 4.14 (b). These defects which were caused during the production of the samples may affect the consistency of the data and the homogeneity of the samples which can affect the isotropic assumption for the tests.

CHAPTER 5

CONCLUSION AND RECOMMENDATION

5.1 Conclusion

The strain energy release rate and the R curve has been determined for the specimens loaded in tension for unidirectional 0˚. The average initiation value obtained was 237.77 kJ/m^2 ± 50.39 and the average propagation value obtained was 15.98 kJ/m^2 ± 0.8. For unidirectional 90˚ samples the R curve was difficult to be plotted since the crack direction was not consistent. The load was much higher than in unidirectional 0˚ because the fibres were parallel to the loading direction. Fibre bridging occurred to both samples.

In compression tests, numerical data was not possible to be obtained since the damage observed was different than the expected. The boundary conditions of the test may be different since the crack propagated away from the fabricated crack tip. Compressive damage such as kink bands were not observed for unidirectional 90˚. Fibre bridging was present in the compressive tests as well.

Visual analysis conducted on the samples indicate that in unidirectional samples, the matrix failure was more apparent. Damages on fibres were little and difficult to be seen. This also proves that with the current fibre volume ratio of 45%, the interface strength is low and therefore fibre debonding occurs for specimen loaded in tension.

5.2 Recommendation

a) To obtain a higher fracture toughness and strain energy, an alternative layup sequence can be proposed for the unidirectional samples which is cross ply.

b) A lower fibre volume ratio will ensure that there is more matrix and expected to have sufficient coating which will allow the matrix to distribute the load to the fibres more effectively.

c) Compare the data with samples manufactured using hand layup as the composite will have more resin and a lower fibre volume ratio can be achieved in this technique.

d) Treatment of the fibres and adding compatibilizer can help to improve the interfacial adhesion properties.

REFERENCES

[1] G. Frossard, J. Cugnoni, T. Gmür and J. Botsis, "Ply thickness dependence of the intralaminar fracture in thin-ply carbon-epoxy laminates," *Composites Part A,* vol. 109, pp. 95-104, 2018.

[2] S. T. Pinho, P. Robinson and L. Iannucci, "Fracture toughness of the tensile aand compressive fibre failure modes in laminated composites," *Composites Science and Technology,* vol. 66, pp. 2069-2079, 2006.

[3] M. J. Laffan, S. T. Pinho, P. Robinson, L. Iannucci and A. J. McMillan, "Measurement of the fracture toughness associated with the longitudinal fibre compressive failure mode of laminated composites," *Composites: Part A,* vol. 43, pp. 1930-1938, 2012.

[4] *ASTM D 5045 : Standard Test Methods for Plane-Strain Fracture Toughness and Strain Energy Release Rate of Plastic Materials,* American Society of Testing and Materials.

[5] P. P. Camanho and G. Catalanotti, "On the relation between the mode I fracture toughness of a composite laminate and that of a 0 ply: Analytical model and experimental validation," *Engineering Fracture Mechanics,* vol. 78, pp. 2535-2546, 2011.

[6] M. S. Prasad, C. S. Venkatesha and T. Jayaraju, "Experimental Methods of Determining Fracture Toughness of Fiber Reinforced Polymer Composites under Various Loading Conditions," *Journal of Minerals & Materials Characterization & Engineering,* vol. 10, no. 13, pp. 1263-1275, 2011.

[7] M. Chabchoub, B. Vieille and R. M. Pitti, "Numerical estimation of the mode I strain energy release rate in woven-ply thermoplastic-based composites at high temperature based on Gθ method," *Theoretical and Applied Fracture Mechanics,* vol. 101, pp. 169-177, 2019.

[8] H. Liu, B. G. Falzon, G. Catalanotti and W. Tan, "An experimental method to determine the intralaminar fracture toughness of high-strength carbon-fibre reinforced composite aerostructures," *Aeronautical Journal,* vol. 122, no. 1255, pp. 1352-1370, 2018.

[9] Z. Khan, B. F. Yousif and M. Islam, "Fracture behaviour of bamboo fiber reinforced epoxy composites," *Composites Part B,* vol. 116, pp. 186-199, 2017.

[10] A. Ortega, P. Maimí, E. V. González and L. Ripoll, "Compact tension specimen for orthotropic materials," *Composites: Part A,* vol. 63, pp. 85-93, 2014.

[11] T. Lisle, C. Bouvet, N. Hongkarnjanakul, M.-L. Pastor, S. Rivallant and P. Margueres, "Measure of fracture toughness of compressive fiber failure in composite structures using infrared thermography," *Composites Science and Technology,* vol. 112, pp. 22-33, 2015.

[12] N. Blanco, D. Trias, S. Pinho and P. Robinson, "Intralaminar fracture toughness characterisation of woven composite laminates. Part II: Experimental characterisation," *Engineering Fracture Mechanics,* vol. 131, pp. 361-370, 2014.

[13] M. Mostafavi, M. J. Schmidt, B. J. Marsden and T. J. Marrow, "Fracture behaviour of ananisotropic polygranular graphite (PGA)," *Materials Science & Engineering A,* vol. 558, pp. 265-277, 2012.

[14] C. Soutis, P. T. Curtis and N. A. Fleck, "Compressive failure of notched carbon fibre composites," *Proceedings of the Royal Society,* vol. 440, pp. 241-256, 1993.

[15] S. Keck and M. Fulland, "Effect of fibre volume fraction and fibre direction on crack paths in unidirectional flax fibre-reinforced epoxy composites under static loading," *Theoretical and Applied Fracture Mechanics,* pp. 162-168, 2019.

[16] M. J. Laffan, S. T. Pinho, P. Robinson and L. Iannucci, "Measurement of the in situ ply fracture toughness associated with mode I fibre tensile failure in FRP. Part I: Data reduction," *Composites Science and Technology*, vol. 70, pp. 606-613, 2010.

APPENDICES

APPENDIX A: Crack Tip Geometry

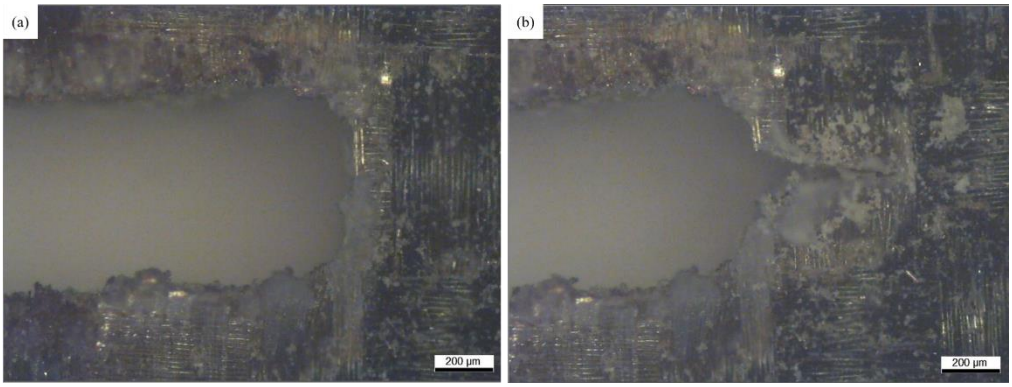

Figure A.1: (a) Saw cut (b) Razor blade sharpened crack tip